

Kinematic Calibration Using a Plane Constraint

Milan Ikits

Dept. of Process Control
Technical University of Budapest
Budapest, Muegyetem Rkpt. 9. H 1111

John M. Hollerbach

Dept. of Computer Science
University of Utah
Salt Lake City, UT 84112

Abstract

This work deals with closed-loop calibration methods where the robot endpoint is constrained to lie on a plane. Previously published calibration approaches are shown to have certain weaknesses. A new solution is given using DH and Hayati notations and standard nonlinear least squares optimization. The procedure is extended via the Implicit Loop Method, which takes input noise into account. Pose selection is guided by the Noise Amplification Index. Simulation and experimental results are presented for a PUMA 560 industrial manipulator, and are compared to those obtained from an open-loop calibration procedure.

1 Introduction

Most kinematic calibration techniques require expensive and/or complicated pose measuring devices, therefore the necessity of developing procedures which use data only from the internal sensors of a robot is evident. This paper presents closed-loop methods which use only one endpoint constraint, i.e., the number of calibration equations per pose is one [6]. Using a probe, the robot touches a number of points on a fixed selected plane, and from the formulated identification model the real robot parameters can be estimated applying an optimization technique.

Three important issues have to be considered in these methods. Like in every closed-loop calibration - not having a priori knowledge about the task constraint - the *scale* of the mechanism must be set, i.e., one link length has to be known [1]. Special care has to be taken about the location of the base and end link frames, which add to the number of identifiable parameters. Finally, we should not ignore the effect of errors in the joint angle measurements. It has been shown that this so-called *input noise* may cause bias in the parameter estimates [9]. Since the end effector is constrained, the input noise is not negligible compared to the output noise. Thus a total least squares optimization procedure is recommended to avoid unreliable estimates [6].

We begin by reviewing previous calibration proposals. After our analysis a new solution is given and examined through both simulation and experiment.

2 Previous Approaches

In recent years several calibration approaches have been proposed that yield only one equation per pose [6]. Open-loop methods include the use of a single wire potentiometer [3], an instrumented ball bar [4], and a laser displacement meter [11]. Closed-loop methods have employed a ball bar with known length [2] and a plane constraint [10, 13]. For the method of planar constraints, two approaches towards formulating an identification model are (1) the use of the general equation of the constraint plane, and (2) the use of plane normals which are supposed to be parallel.

2.1 Using the Equation of the Plane

The most straightforward approach assumes that the endpoints satisfy the plane equation:

$$ax_c^i + by_c^i + cz_c^i = [a \ b \ c] p_c^i = 1 \quad (1)$$

where $i = 1, \dots, P$ for P poses, and a , b , and c are the generalized plane coefficients. This equation assumes the plane does not intersect the origin.

The computed endpoint positions p_c^i deviate from the plane due to errors from the kinematic model and the measurements. To reduce these deviations, we minimize

$$S = \sum_{i=1}^P ([a \ b \ c] p_c^i - 1)^2 \quad (2)$$

where the expression in the brackets is proportional to the distance of p_c^i from the plane.

The computed endpoint positions are a nonlinear function of the robot parameters ϕ and the joint angles ϑ^i :

$$p_c^i = f^i(\phi, \vartheta^i) = f^i(\phi) \quad (3)$$

where the joint angle inputs have been folded into f . After substitution into (2), we get the objective function of the nonlinear optimization problem:

$$S = \sum_{i=1}^P ([a \ b \ c] f^i(\phi) - 1)^2 = \sum_{i=1}^P (g^i(a, b, c, \phi) - 1)^2 \quad (4)$$

where ϕ contains the robot parameters, which are defined by a certain kind of parameterization including joint angle

offsets γ_j too. This parametrization has to choose appropriate coordinate frames; the plane, the robot mechanism, and a tool transform are included in the parametric function g . One could continue with calculating the Jacobian and applying for example Gauss-Newton optimization, but we have found this overall approach deficient.

Consider the calibration of a two link planar manipulator using a line constraint. This two dimensional version of the 3D plane calibration method shows the deficiency of this approach easily. The objective function can be expressed similarly except that f^i has only two components. One link length has to be fixed and the first joint angle offset γ_1 is not identifiable.

Using *Matlab*TM we generated 40 points on a line uniformly. After adding Gaussian noise we calculated the joint angle readings by solving the inverse kinematics of the manipulator. The deviations from the real and calibrated lines using the parameters obtained from the calibration based on the approach above are shown in Figure 1. It can be seen that using the identified kinematic model the endpoints do not fit the original line ($dvr = 0$ mathematically). Instead they fit a different line (which is defined by the calibrated line coefficients).

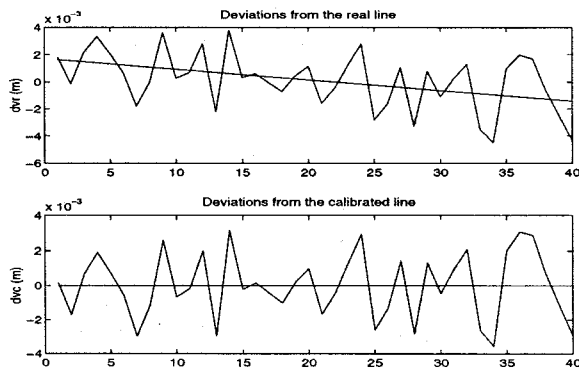


Figure 1: Deviations from the real and calibrated lines.

The reason is that the definition of the base frame is wrong; we have to fix the base frame to the line and not to the first robot axis. It also can be seen that the deviations fit the calibrated line perfectly. The situation is similar in the three dimensional case; the calibration plane “wanders.”

2.2 Using Plane Normals

This approach is based on the calculation of the vector products of a set of difference vectors in the same plane, which are supposed to yield plane normals [13]. Three points determine a plane, and yield two independent difference vectors from which the plane normal can be extracted. From the cross products of these “small plane” normals a linear identification equation system can be derived. Besides the definition of the base frame, this method has two more problematic aspects:

- We have to be careful with the pose selection because we can get collinearities — which make the identification difficult — very easily.
- Not all the points are considered in the identification at a time, only a set of points is used. If we wanted to include all the points, the Jacobian would be huge.

These aspects are independent of where we place the constraint plane. Because this approach does not even use a numerical description of the plane (it only assumes that the endpoints are lying on *some* plane), we found that the wandering-effect occurs more seriously.

3 A Regular Approach

To make the 3D plane calibration method work, we found that a careful definition of the base frame was essential.

3.1 The Kinematic Model

Every kinematic model includes geometric and non-geometric parameters of the robot. For the geometric parameters typically four-parametric models are used. We use the well-known DH notation for nearly perpendicular neighboring axes, and Hayati parameterization [5] in the nearly parallel case. We give the definition of the metrology or base frame and the end link frame exclusively; the definition of the intermediate frames can be found in for example [7]. The non-geometric parameters include only the joint offsets, since in most closed-loop calibration methods the gains are difficult to estimate [6].

3.1.1 Definition of the Base Frame

There are two cases for the definition according to whether the first robot axis is parallel with or perpendicular to the plane. We show the definition for the first case using DH parameters.

In order to handle the problem easier, let’s number the base frame as -1 (Figure 2). There is a problem with finding frame origins O_0 and O_{-1} , because there is no constraint on the location of the endpoint on the plane. Assuming that we can apply DH parameters for frame 1, the first definitive point is the intersection of the common normal x_1 with the first rotation axis z_0 . This intersection is a good choice for O_0 , which then sets $d_1 = 0$.

Project O_0 to the plane to set O_{-1} and z_{-1} . Since the first robot axis is nearly parallel to the plane, z_{-1} and z_0 are nearly perpendicular, and their common normal x_0 is well defined. Set x_{-1} equal to x_0 , which fixes $a_0 = 0$ and $\gamma_0 = 0$. Note that we use two parameters between frames 0 and 1, and three parameters between frames -1 and 0.

When the first robot axis is nearly perpendicular to the plane, we can use Hayati parameters. The intersection of the plane and the first robot axis defines O_0 . Working backwards we get that $a'_0 = 0$, $\gamma'_0 = 0$ and $\gamma'_1 = 0$. However

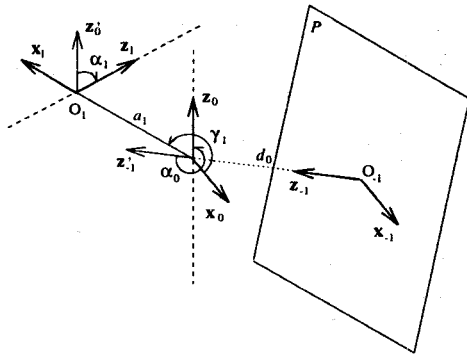


Figure 2: Base coordinates.

we noticed that this configuration yielded a serious observability problem in case of the Puma 560 robot.

3.1.2 Definition of the End Link Frame

Because the orientation of the end link frame does not play a role, only three parameters out of the four are needed. We can choose z_n to be parallel with z_{n-1} ; this sets $\alpha_n = 0$.

3.2 The Identification Procedures

3.2.1 Nonlinear Least Squares Optimization

Relative to the -1 frame (Figure 2), the plane constraint on the end link frame can be expressed by the calibration equation:

$$p_z^i = 0$$

After substituting the forward kinematics (3) of the robot and linearizing the equation, we get:

$$\Delta p_z^i = 0 - \hat{f}^i(\phi^k) = \hat{C}^i \Delta \phi$$

where \hat{f}^i contains the third component of f^i . This equation is the basis for the iterative update of parameters.

3.2.2 Implicit Loop Method

The Implicit Loop Method is based on the unification of open and closed-loop methods: the closure of kinematic loops by end-effector measurements or by constraints are considered equivalent [12]. All kinds of measurement errors are included implicitly in the loop equations:

$$f(x_i, \phi) = f(\bar{x}_i + \hat{x}_i, \bar{\phi} + \hat{\phi}) = 0, \quad i = 1, \dots, P \quad (5)$$

where \bar{x}_i contains the measurements (both input and output) taken at pose i with measurement error \hat{x}_i , and $\bar{\phi}$ is the initial estimates of the parameters which have errors of $\hat{\phi}$. The goal is to find the most likely combination of parameter errors $\hat{\phi}$ and measurement noises \hat{x}_i which satisfy the loop equations. Assuming Gaussian noise with zero mean,

the maximum likelihood estimate is obtained by minimizing the following chi-square function:

$$\chi^2 = \sum_{i=1}^P (\hat{x}_i^T \Sigma_x^{-1} \hat{x}_i + \hat{\phi}^T \Sigma_\phi^{-1} \hat{\phi}) \quad (6)$$

where Σ_x and Σ_ϕ are the covariance matrices of the measurement errors and the parameters, respectively. Iteratively minimizing this sum subject to (4), one could get estimates for errors in both the kinematic parameters and the measurements.

The inclusion of the covariance matrices means that we use some *a priori* knowledge about the error distributions. Thus the method puts parameter variations, joint and end-effector measurements on equal footing. Since the loop equations are satisfied exactly, no equation scaling is needed. Besides these advantages, the approach provides measures for both the accuracy of the fitted parameters and the consistency of the data with the model analytically. The accuracy of the estimated parameters ϕ^* compared to their actual values ϕ is zero mean with covariance

$$\Sigma_\phi^* = \Sigma_\phi^{-\frac{1}{2}} \Sigma_q \Sigma_\phi^{\frac{1}{2}} \quad (7)$$

where subscript $\frac{1}{2}$ denotes the symmetric square root, and Σ_q can be derived from the procedure.

The method also provides a measure as to whether the results of the estimation agree with the statistical assumptions of the model. Substituting the converged values, the χ^2 function can be approximated by a Gaussian distribution with expected value of PC and standard deviation of $\sigma = \sqrt{2PC}$, where C is the number of calibration equations per pose. The complete formulation of the Implicit Loop Method can be found in [12].

4 Simulation Results

In the simulations we generated joint angle readings by solving the inverse kinematics of the Puma robot from endpoints on a given plane. The endpoints were selected according to grid or random distributions and Gaussian noise was added with given variances in directions x, y and z . The nominal parameters of the Puma robot can be found in Table 1 along with the base and end link parameters. The a_6 offset of the touching probe was built intentionally to make the last joint offset observable.

4.1 Pose Selection

In order to achieve accurate estimates the robot should be positioned into an appropriate pose set. Here we use the noise amplification index [7] - which is the ratio of maximum singular value to condition number - as the indicator of how many samples in what arrangement should be collected. The bigger this number is the smaller the errors in the identified parameters are.

j	γ_j (deg)	d_j (mm)	a_j (mm)	α_j (deg)	β_j (deg)
0	0	740.0	0	90.0	0
1	0.0	0	0.0	-90.0	0
2	0.0	0	431.8	0.0	0.0
3	0.0	149.09	-20.32	90.0	0
4	0.0	433.07	0.0	-90.0	0
5	0.0	0.0	0.0	90.0	0
6	0.0	175.25	-12.0	0	0

Table 1: Nominal parameters of the Puma 560 robot. Defined zero parameters are indicated as 0.

Figure 3 shows the results of the simulation; 5000 poses were generated according to random distribution on a plane. From this pose set 50 to 300 poses were selected randomly and the corresponding indices were calculated. The result is a distribution with a large variance, because not only the number, but also the location of the poses matters. From fitting a curve on this distribution and examining the tendency, a sufficient number of poses can be inferred.

The default number of poses is 50. While adding from one to 100 more poses the noise amplification index increased significantly; from 150 poses it did not change much. However we should not ignore the human factors: the collection of 150 poses is a tedious procedure. Taking this factor into account we chose 120 as the “optimal” number of poses. Another issue is the location of the samples. The simulations showed that collecting poses according to a rectangular grid yields a bigger noise amplification index. Therefore the selection of 96 poses was based on an 8-by-12 grid and the remaining 24 poses were collected randomly.

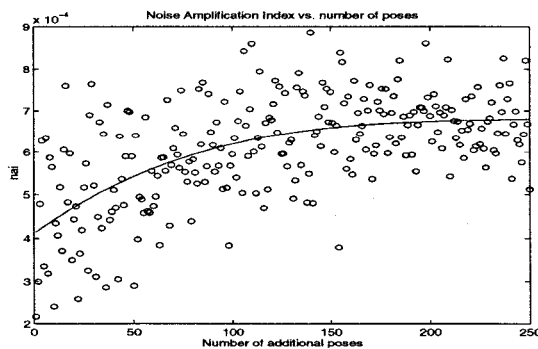


Figure 3: Pose selection using the noise amp. index.

5 Experimental Results

In order to cross-check the improved accuracy of the calibrated manipulator, two calibrations were performed simultaneously. Besides taking 120 poses on a plane with the touching probe, 60 position measurements using the Optotrak 3D motion tracking system (Northern Digital Inc.,

Waterloo, Ontario) were collected too. Thus the results of the open loop calibration could be compared to the results of plane methods, and helped with choosing a known link length.

5.1 Open Loop Calibration Using Position Measurements

An open loop calibration procedure was applied using Gauss-Newton optimization, and the RMS error between the measured and predicted endpoints was reduced to 0.156 mm. This result corresponds to the accuracy of the Optotrak, which is stated to be 0.1 mm at a viewing distance of 2.5 m.

We have to be careful with the cross-check because in this case the setup of the base and end link frames is different from the setup described before. Also the Optotrak calibration determines 27 parameters while the plane version yields only 23. Therefore the cross-check is performed by substituting the internal parameters of the open loop results to the closed loop calibrated parameters. Using this mixed set and the calibration results of the closed loop method, two pose sets can be generated. The inter-distance of any two points in the two sets are compared and the RMS error of these distances are calculated taking each pair into account.

Another problem is the scaling of the mechanism in the closed loop methods: we have to fix one link length. It seems reasonable to choose this parameter from the Optotrak results. To verify this statement we repeated the open loop calibration using the Implicit Loop Method. By setting $\Sigma_\phi \rightarrow \infty$ (numerically this means 10^5 times of its normal value) and the standard deviation of the input noise to zero, we could reconstruct the estimates of the Nonlinear Least Squares method. The reconstruction gave a $\chi^2 = 110.6$ with an expected value of $P \times C - N = 153$ (where N denotes the number of parameters). This is a little bit low but within the acceptable 99% region, and because of that we set the variance of the output noise double the precision of the Optotrak (0.2 mm).

From the internal parameters we had to choose from two candidates for the fixed link length (a_2 or d_4). The standard deviation of the errors between the real and calibrated parameters were calculated (from the diagonal entries of covariance matrix Σ_ϕ^* - see (6)). Link length parameter a_2 had a smaller standard deviation of parameter error ($\sigma_{a_2} = 0.0677mm$) than d_4 ($\sigma_{d_4} = 0.0876mm$), so it seemed reasonable to consider it as a known parameter (very close to the real value). However to see the difference three closed loop calibrations were performed each time; one with fixed link length a_2 , another with fixed d_4 , and a third one when both of them were fixed.

Fixed par.	Condition Number	Noise Amp. Index	RMS Err. of Dist. (mm)
d_4	58.35	7.06×10^{-4}	0.865 ; 0.799
a_2	74.89	4.24×10^{-4}	0.746 ; 0.780
Both	54.32	7.72×10^{-4}	0.269 ; 0.325

Table 2: Comparison of closed loop calibrations.

5.2 Closed Loop Calibrations Using a Plane Constraint

The results of the comparison are shown in Table 2. Only 100 measurements were used for calibration; the remaining 20 poses could be used for independent test. To see the robustness of the model and the procedure, we list the condition numbers and noise amplification indices too. The RMS errors of the cross-check are included for the calibration and the test pose set respectively.

Interestingly the best results were obtained when both candidates were fixed. However, this makes the planar calibration unreasonable. Although for d_4 the condition number of the Jacobian is larger (probably because a_2 has better observability and this makes the procedure more robust), the final results of the cross-check are worse. Thus we chose a_2 as the known link length.

The identified parameter errors (w.r.t. the nominal PUMA parameters), obtained by setting $a_2 = 432.3mm$ from the Optotrak results, are collected into Table 3. The huge joint angle offsets γ_j are due to the zero level of the potentiometers in the joint angle sensors not having been set correctly. The RMS error of the endpoint distances from the plane was reduced to 0.2515 mm w.r.t. the 100 test points and to 0.2774 mm for the independent 20 test points.

It is of interest whether we can build a better model by taking the input noise into account. First using all the 120 points we replicated the NLS method by setting $\Sigma_\phi \rightarrow \infty$, the standard deviation of the output noise $\sigma_\epsilon = 0.25mm$, and the standard deviation of the input noise $\sigma_\psi = 0$. We got back the same parameter corrections, results and a χ^2 value of 120.3 which is a little bit far from its expected value $P \times C - N = 97$ but in the acceptable region.

Then to deal with joint sensor noise, we modified the model by including input noise standard deviation of $\sigma_\psi = 0.1mrad$. This seems reasonable because it can cause errors in the endpoints having standard deviation of 0.1 mm. The optimization yielded a χ^2 value of 134.7 with expected value of $P \times C = 120$. The initial estimates were modified to match the a priori standard deviation of parameter errors which was set to 0.002 (rad,m). Performing the cross check with the mixed parameter set yielded the RMS error between inter-distances of 0.5303 mm.

j	$\hat{\gamma}_j$ (deg)	\hat{d}_j (mm)	\hat{a}_j (mm)	$\hat{\alpha}_j$ (deg)	$\hat{\beta}_j$ (deg)
0	0	5.27	0	-4.963	0
1	-3.439	0	0.27	0.021	0
2	7.028	0	0	0.104	-0.275
3	-2.693	1.19	-0.67	0.04	0
4	-6.932	-2.03	0.06	0.0225	0
5	-1.749	-0.19	-0.01	0.008	0
6	-14.331	-0.4	-0.7	0	0

Table 3: Identified errors in the parameters.

5.3 Statistical Analysis

The results of the error analysis of the fitting processes are shown in Table 4. The standard deviations of the errors between the estimated and real parameters are calculated from the diagonal elements of Σ_ϕ^* . Huge uncertainties are found among the last two joint angle offsets and skew angles. One reason for this might be backlash in the Puma wrist, noticed during the experiment too, which can cause outliers and make the Gaussian assumption of joint sensor errors invalid. It is shown that link lengths d_{3-6} might be far from the real values too.

Parameter	NLS (mrad,mm)	ILM (mrad,mm)
γ_1	0.0907	0.0904
γ_2	0.2034	0.1985
γ_3	0.6604	0.6205
γ_4	0.6621	0.5897
γ_5	3.4756	1.7146
γ_6	7.8142	1.9379
α_0	0.2131	0.2088
α_1	0.3389	0.3352
α_2	0.1758	0.1756
α_3	0.7979	0.7321
α_4	1.7140	1.2930
α_5	3.7753	1.7514
β_2	4.2423	4.1051
a_1	0.0558	0.0561
a_3	0.2975	0.2795
a_4	0.0557	0.0520
a_5	0.6141	0.3143
a_6	0.0818	0.0774
d_0	0.5389	0.5042
d_3	3.2211	3.0269
d_4	3.3906	3.1569
d_5	6.4105	3.2808
d_6	4.2362	4.0878

Table 4: Standard deviations of parameter errors.

These discrepancies can also be explained from a different viewpoint. It has been shown in [12] that considering the singular value decomposition of the augmented Jacobian $\hat{D} = U\Sigma V^T$, the columns of V are independent error directions having standard deviations $\hat{\sigma}_i = 1/\sqrt{\sigma_i^2 + 1}$.

When the measurements are noisy, or when the model is not complete, some parameters are hardly observable; σ_i will be small and $\hat{\sigma}_i$ will remain at its original value of 1 leaving the estimates unchanged from the initial values. Otherwise it will be reduced to approximately $1/\sigma_i$, i.e., the estimated parameter will be close to the real value. By examining the singular values of the ILM Jacobian we could calculate that the final parameter errors were reduced to 0.77% and 69.63% of the initial value for the best and worst directions, respectively.

6 Conclusions

Calibration using a planar constraint is the most significant remaining closed-loop approach to be developed. We found that it was surprisingly difficult to develop a viable approach. Previous proposals for formulations using the plane equation or using normals obtained from cross products of difference vectors were found problematical. For example, the fitted plane wandered, even though the resulting parameters matched to it well. The key for us was a careful definition of the base frame, by a projection back from the first distinctive axis intersection point on the mechanism to the plane.

Good results were obtained with proper definition of the base and end link frames. The results of two optimization techniques, Nonlinear Least Squares Optimization and the Implicit Loop Method, were compared. NLS Optimization is easy to implement, but is based on the reduction of output noise only. Among the advantages of the Implicit Loop Method is that a priori information about parameter and measurement errors can be included easily. The applied model can be verified and unmodeled factors are uncovered by the statistical analysis.

The experimental results showed that this method is suitable for robot calibration without using external sensors, though unmodeled factors and the fact that we use only one calibration equation per pose can cause observability problems with the parameters. Special care has to be taken about the location of the constraint plane and the points selected for calibration.

Acknowledgments

Support for this research was provided by NSF Grant MIP-9420352 and NSERC NCE IRIS Project HMI-8.

References

- [1] Bennett, D.J., and Hollerbach, J.M., "Autonomous calibration of single-loop closed kinematic chains formed by manipulators with passive endpoint constraints," *IEEE Trans. Robotics and Automation*, 7, 1991, pp. 597-606.
- [2] Driels, M.R., 1993. "Using passive end-point motion constraints to calibrate robot manipulators," *J. Dynamic Systems, Meas., Control*, 115, pp. 560-565.
- [3] Driels, M.R., and Swayze, W.E., 1994. "Automated partial pose measurement system for manipulator calibration" *IEEE Trans. Robotics and Automation*, vol 10., pp. 430-439
- [4] Goswami, A., Quaid, A., and Peshkin, M., 1993. "Identifying robot parameters using partial pose information," *IEEE Control Systems*, 13, no. 5, pp. 6-14.
- [5] Hayati, S.A., and Mirmirani, M., 1985. "Improving the absolute positioning accuracy of robot manipulators," *J. Robotic Systems*, 2, pp. 397-413.
- [6] Hollerbach, J.M., and Wampler, C.W., "The calibration index and taxonomy of kinematic calibration methods," *Intl. J. Robotics Research*, 14, 1996, pp. 573-591.
- [7] Mooring, B.W., Roth, Z.S., and Driels, M.R., 1991. *Fundamentals of Manipulator Calibration*, NY, Wiley Interscience.
- [8] Nahvi, A., and Hollerbach, J.M., 1996. "The noise amplification index for optimal pose selection in robot calibration," *Proc. IEEE Intl. Conf. Robotics and Automation*, Minneapolis, April 22-28, pp. 647-654.
- [9] Norton, J.P., 1986. *An Introduction to Identification*, London, Academic Press.
- [10] Tang, G.-R., 1986. *Calibration and Accuracy Analysis of a Six-Axis Industrial Robot*, Ph.D. thesis, Texas A&M Univ. Dept. Mechanical Engineering.
- [11] Tang, G.-R., and Liu, L.-S., 1993. "Robot calibration using a single laser displacement meter," *Mechatronics*, 3, pp. 503-516.
- [12] Wampler, C.W., Hollerbach, J.M., and Arai, T., 1995. "An Implicit Loop Method for kinematic calibration and its application to closed-chain mechanisms," *IEEE Trans. Robotics and Automation*, 11, pp. 710-724.
- [13] Zhong X.-L., and Lewis J.M., 1995. "A new method for autonomous robot calibration," *Proc. IEEE Int. Conf. Robotics and Automation*, Nagoya, May 21-26, pp. 1790-1795.